Biosensors and Bioelectronics 141 (2019) 111452

Contents lists available at ScienceDirect

Biosensors and Bioelectronics

journal homepage: www.elsevier.com/locate/bios

An acetylcholinesterase biosensor based on doping Au nanorod@SiO_2 nanoparticles into TiO2-chitosan hydrogel for detection of organophosphate pesticides

Hui-Fang Cui*, Ting-Ting Zhang, Qi-Yan Lv, Xiaojie Song, Xiao-Jing Zhai, Gai-Gai Wang

Department of Bioengineering, School of Life Sciences, Zhengzhou University, 100# Science Avenue, Zhengzhou, 450001, PR China

ARTICLE INFO

Keywords:
Au nanorods
Mesoporous SiO_2
Organophosphorus pesticides detection
Acetylcholinesterase biosensor
TiO_2
Chitosan

ABSTRACT

A stable and sensitive electrochemical acetylcholinesterase (AChE) biosensor for detection of organophosphorus pesticides (OPs) was developed by doping Au nanorods (AuNRs)@mesoporous SiO_2 (MS) core-shell nanoparticles into CS/TiO_2-CS (CS denotes for chitosan) immobilization matrix. AuNRs@MS core-shell nanoparticles were synthesized and characterized. The doping and the biosensor fabrication process were probed and confirmed by scanning electron microscopy and electrochemistry techniques. The doping conditions were optimized. The matrix both before and after AChE immobilization had a mesoporous nanostructure. The nanoparticles dispersed homogeneously within the matrix. The doping significantly enhanced the electroconductivity of the TiO_2-CS hydrogel, and dramatically improved the bioelectrocatalytic activity and OPs detection sensitivity of the AChE immobilized matrix. The detection linear ranges for both dichlovos (DDVP) and fenthion were from 0.018 μM (4.0 ppb) to 13.6 μM, and the limit of detection (LOD) was 5.3 nM (1.2 ppb) and 1.3 nM (0.36 ppb), respectively. The biosensor exhibited high reproducibility and accuracy in detecting OPs spiked vegetable juice samples. In addition, it exhibited very high detection stability and storage stability. The developed AChE biosensor was provided to be a promisingly applicable tool for OPs detection with high reliability, simplicity, and rapidness.

1. Introduction

Organophosphorus pesticides (OPs) are a kind of phosphorus-containing synthetic pesticides. Being widely used to protect crops from insects, most OPs are wide-spectrum, low resistance production, and safety to crops (Mostafalou and Abdollahi, 2017), However, OPs are toxic to human and most animals. They can cause the damage of nervous system through inhibition of acetylcholinesterase (AChE), the enzyme in neurosynapses (Patocka et al., 2004; Costa, 2006; Eddleston et al., 2008). Detection of OPs in various samples with high reliability, simplicity, and rapidness has become increasingly necessary.

In the past decades, people have endeavored to develop efficient and simple methods to determine OPs levels (Long et al., 2015; Lu and Xia, 2015; Qian and Lin, 2015; Yu et al., 2015). Among them, electrochemical biosensors have stood out due to their high reliability, simple instruments, fast result-acquisition, easy operation, high sensitivity, and compatible to complex samples. The working mechanism of electrochemical OPs biosensors depends on the AChE catalytic production of electro-active thiocholine (TCl) from the substrate acetylthiocholine (ATCl) (Yu et al., 2015; Wei and Wang, 2015). Inhibition of the AChE activity by OPs would result in reduced production of TCl, thus the decrease of the electrochemical signal output. It is obvious that the property of enzyme immobilization matrix plays a key role in development of practically applicable electrochemical biosensors. An ideal immobilization matrix should be stable, porous, electro-conductive, hydrophilic, biocompatible, positively-changed, electrocatalytic to TCl, and high-contact to solid substrates. With an ideal immobilization matrix, firstly, AChE (a negatively-charged enzyme) could be effectively immobilized while maintaining its native catalytic activity. Secondly, small molecules, including ATCl, TCl, and OPs could easily transport through the matrix and efficiently contact with the immobilized enzyme. In addition, the enzymatic product TCl could be electro-catalytically oxidized. Last but not the least, the biosensor could be stable in applications and in storage.

In recent years, the advances in nanotechnology have provided various nanomaterials with special properties, such as high specific surface area and high electrocatalytic activity, for fabrication of AChE electrochemical biosensors (Wei and Wang, 2015; Shi et al., 2006;

* Corresponding author.
E-mail address: hfcui@zzu.edu.cn (H.-F. Cui).

https://doi.org/10.1016/j.bios.2019.111452
Received 19 March 2019; Received in revised form 18 June 2019; Accepted 19 June 2019
Available online 22 June 2019
0956-5663/

Sundarmurugasan et al., 2016). However, most of the reported AChE electrochemical biosensors still face instability problems. Fortunately, a highly stable AChE biosensor for detection of OPs has been developed in our group simply by adsorption of AChE on chitosan (CS) film modified TiO_2-CS hydrogel (denoted as CS/TiO_2-CS) (Cui et al., 2018). The CS-TiO_2 as well as the TiO_2 hydrogel can be formed in-situ from their corresponding precursor colloidal solution immediately after being cast on electrode surfaces, resulting in a very good contact with the electrode surfaces. Additionally, the hydrogel films have a mesoporous nanostructure, possessing many advantageous properties, such as large specific surface area, low cost, non-toxicity, good thermal and chemical stability, and excellent biocompatibility (Cui et al., 2013, 2018; Yu and Ju, 2002; Zhu et al., 2009). Furthermore, blending CS into and modifying a CS film onto the TiO_2 hydrogel have been proved effective strategies to reinforce the mechanical strength of the TiO_2 sol-gel (Cui et al., 2018; Behera et al., 2017; Tang et al., 2016; Yang et al., 2017), and increases its AChE loading efficiency (Cui et al., 2018). CS is a biocompatible, adhesive, and positively charged polymer, being used extensively as an enzyme immobilization matrix material in biosensor fabrications (Ma et al., 2018; Varmira et al., 2018). However, the electro-conductivity and electrocatalytic activity of the CS/TiO_2-CS immobilization matrix need to be improved to enhance the electro-oxidation signal of the enzymatic product (TCl). With this improvement, the OPs detection sensitivity of the AChE biosensor should be further improved.

Au nanoparticles have many unique properties such as facile synthesis, easy for surface modification, excellent biocompatibility, high photostability, surface plasmon resonance property, high electro-conductivity, high electrocatalytic activity, and strong anti-oxidation ability (Nam et al., 2004; Hill et al., 2007; Li et al., 2009; Cui et al., 2015). Among various morphologies of Au nanoparticles, Au nanorods (AuNRs) have been studied extensively for biomedical applications due to their superior tunable optical properties, high scattering cross sections, and core-shell nanostructure forming ability with mesoporous silica (MS) (Choi et al., 2012; Wang et al., 2005; Fang et al., 2016; Chang et al., 2012). The MS shell can provide porous, high surface area, and biocompatible nanostructure for pharmaceutical cargo delivery (Fang et al., 2016; Chang et al., 2012), while the AuNRs core can serve as a two-photon photoluminescence (TPL) bright contrast agent for TPL imaging (Fang et al., 2016), and an absorbent of NIR light for photothermal therapy of cancers (Fang et al., 2016; Chang et al., 2012).

In this study, we investigated the effect of doping AuNRs@MS core-shell nanoparticles into the TiO_2-CS hydrogel on the electro-conductivity and electrocatalytic activity of the gel matrix, and on the OPs detection sensitivity of the AChE biosensor (Scheme 1). To our knowledge, AuNRs@MS nanoparticles have not been reported in biosensor fabrication. The MS shell was expected to protect the AuNRs from aggregation, while its porous structure should allow the transport of ions, ensuring the enhancement effect of AuNRs on the electro-conductivity and electrocatalytic activity. In addition, small molecules should be able to permeate through the MS shell, to assure the contact of TCl with the electrocatalytic AuNRs. The AChE biosensor fabrication procedures were characterized and optimized. The mechanism of electrocatalytic activity enhancement was investigated and proposed. By taking dichlorvos (DDVP) and fenthion as model OPs, the performances of the biosensor in OPs detection were evaluated and compared with those of our previously developed AChE biosensor (Cui et al., 2018), some other AChE biosensors (Wei and Wang, 2015; Sundarmurugasan et al., 2016; Itoh et al., 2014; Guan et al., 2012; Yan et al., 2013; Kaur et al., 2015; Dutta and Puzari, 2014; Wu et al., 2013), and some traditional detection methods (Santos et al., 2018; Radišic et al., 2009; Srivastava et al., 2017; Navarro et al., 2013; Qian et al., 2009). Finally, the sensitive, simple, and highly stable AChE biosensor was evaluated for applications in OPs detection in vegetable samples.

2. Experimental

2.1. Materials and chemicals

Acetylcholinesterase (AChE) (from electric eel) and acetylthiocholine (ATCl) were from Sigma-Aldrich. Chitosan (CS) (viscosity > 400 mPa s), dichlorvos (DDVP) (analytical standard, 1 mg mL^{-1} in methanol) and fenthion (analytical standard, 1 mg mL^{-1} in methanol) were from Aladdin Bio-Chem Technology (Shanghai, China). Hydrogen tetrachloroaurate (III) hydrate, $AgNO_3$, and tetraethylorthosilane (TEOS) were purchased from Alfa Aesar (Massachusetts, U.S.A.). Other remaining chemicals were obtained from Sinopharm Chemical Reagent (Shanghai, China). All chemicals if not specified were of analytical grade and used as received. Purified nitrogen with a purity of 99.99% was obtained from Zhengzhou Keyi Industrial Gas (China). Deionized water obtained from a Millipore water system was used throughout the experiment.

2.2. Apparatus and measurement

The glassy carbon (GC) electrode surfaces with various modifications were probed by scanning electron microscopy (SEM, JEOL JSM-7500F), and also characterized by cyclic voltammetry (CV) and electrochemical impedance spectroscopy (EIS) techniques. AuNRs and

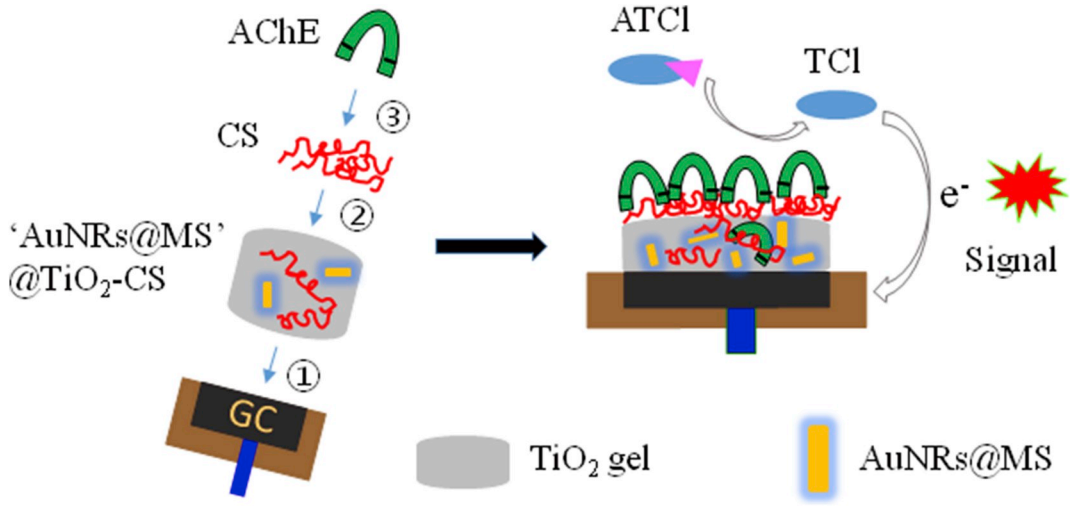

Scheme 1. Schematic illustration of the fabrication steps and the structure of the AuNRs@MS nanoparticles doped AChE biosensor, and its working mechanism to ATCl.

AuNRs@MS nanoparticles were observed by transmission electron microscopy (TEM, FEI Tecnai G2 20, operated at 200 kV), and also characterized by UV–Vis spectroscopy (UV-2450, Shimadzu Scientific Instrument, Japan). The CVs were performed in 0.01 M phosphate buffer solution (PBS, pH 7.4), or in 5 mM $K_3[Fe(CN)_6]$ supported by 1 M KCl. The EIS measurement was executed in 0.1 M KCl containing equimolar $[Fe(CN)_6]^{3-/4-}$ (10/10 mM) with AC frequency from 0.1 Hz to 100 kHz. All electrochemical measurements were performed at room temperature (~25 °C) using a CHI-660E electrochemical work station (Shanghai Chenhua Instrument, China) in a three electrode arrangement consisting of a working electrode (modified GC electrode), a Pt counter electrode and an Ag|AgCl|KCl (3 M) reference electrode.

2.3. Synthesis of AuNRs and AuNRs@MS nanoparticles

AuNRs were synthesized according to the well-developed seed-mediated growth method (Fang et al., 2016; Nikoobakht and El-Sayed, 2003). The procedures are described in detail in the Supplementary Material. Briefly, an Au seed solution was firstly produced from cetyltrimethylammonium bromide (CTAB), $HAuCl_4$, and $NaBH_4$. A growth solution was prepared from $AgNO_3$, CTAB, $HAuCl_4$, H_2SO_4, and ascorbic acid. The growth of AuNRs was then immediately initiated by quickly injecting the seed solution into the growth solution under stirring at 30 °C. Finally, the solution was kept at 30 °C overnight to produce AuNRs.

MS shell was synthesized on AuNRs core according to the modified Stöber method (Varmira et al., 2018). The procedures are described in the Supplementary Material. The resulting AuNRs@MS nanoparticles were dispersed in water. The AuNRs concentration was estimated based on its longitudinal plasmon band absorbance and the absorption coefficient (ξ) for AuNRs of 4.1 aspect ratio ($\xi = 5.2\,nM^{-1}\,cm^{-1}$) (Orendorff and Murphy, 2006).

2.4. Preparation of AuNRs@MS doped TiO_2-CS sol-gel

We have reported the preparation of TiO_2 sol-gel from tetra-n-butyltitanate (Cui et al., 2013, 2018). The hydrogel was formed in minutes from its precursor solution upon exposure a thin layer of the solution to air. The synthesis of the TiO_2 precursor solution was described in detail in the Supplementary Material. The AuNRs@MS doped TiO_2-CS (denotes as 'AuNRs@MS'@TiO_2-CS) hydrogel was similarly formed from its precursor mixture solution. The mixture solution was prepared right before usage by mixing 445.5 μL TiO_2 precursor solution with 49.5 μL AuNRs@MS nanoparticle solution and 5 μL 0.5% CS solution.

2.5. Fabrication of the biosensor

The GC electrode was cleaned by being polished consecutively with 0.3 and 0.05 μm alumina powder and then sonicated in water bath. After dried with N_2 gas blow, the GC electrode was coated with 4 μL 'AuNRs@MS'@TiO_2-CS precursor mixture solution, and then left in the air for gelation. The volume ratio of the TiO_2 precursor solution to the AuNRs@MS solution in mixing was varied from 92:8 to 86:14, and the AuNRs@MS concentration was varied from 0.19 nM to 0.96 nM (based on the AuNRs concentration), to obtain an optimum biosensor. A CS layer was then electrodeposited on the 'AuNRs@MS'@TiO_2-CS/GC surface by holding the potential at −2.5 V for 20 s in 0.2% CS. Finally, AChE was immobilized on the CS/'AuNRs@MS'@TiO_2-CS/GC electrode by dropping 4 μL 5 mg mL^{-1} AChE solution (in 0.01 M PBS) onto the electrode surface. The as-fabricated enzyme electrode was dried in the air and kept at 4 °C, ready for use.

2.6. Bioelectrocatalytic activity and sensing performances

The bioelectrocatalytic activity of the AChE biosensor was investigated by using differential pulse voltammetry (DPV) technique. The DPV was run in 0.01 M PBS containing a series of different concentrations of ATCl (from 0.2 to 1.0 V; amplitude, 0.05 V; pulse width, 0.005 s; pulse period, 0.02 s). Before the DPV measurement, the enzyme electrode was cleaned by running CVs in PBS until a stable CV curve was obtained, to remove loosely adsorbed AChE. The sensing performances were evaluated by recording DPVs in 0.01 M PBS containing 1 mM ATCl before and after incubating the electrode in OPs solution for 10 min at room temperature. The sensing signal towards OPs, which was the inhibition ratio (Inh%) of OPs to the enzyme electrode, was determined from Eq. (1), where $I_{cat}{}^0$ and I_{cat}' represents the DPV peak current in response to 1 mM ATCl before and after the OPs incubation, respectively.

$$Inh\% = (1 - I_{cat}'/I_{cat}{}^0) \times 100\% \quad (1)$$

The detection stability was evaluated by repetitively recording the DPVs in 1 mM ATCl. The storage stability was evaluated by monitoring the DPVs in 1 mM ATCl every 10 days during a wet storage in sterilized PBS at 4 °C, or a dry storage at −20 °C, for 30 days.

2.7. Detection of OPs in vegetable samples

The applicability of the AChE biosensor was evaluated by detecting the fenthion levels in fenthion spiked cabbage juice samples. For preparation of the juice samples, 100 g cabbage pieces were mixed with 100 mL PBS (0.02 M, pH 7.4) in a homogenizer at room temperature. The cabbage homogenate was then centrifuged at 5000 rpm for 10 min. The supernatant was taken as the cabbage juice. The biosensor was incubated with the fenthion spiked cabbage juice samples for 10 min, and then subject to DPV detection in 1 mM ATCl. The Inh% values were compared with the calibration curve to obtain the found OPs concentration.

3. Results and discussion

3.1. Characterization of AuNRs and AuNRs@MS nanoparticles

AuNRs were prepared according to the seed-mediated growth method (Fang et al., 2016; Nikoobakht and El-Sayed, 2003). The aspect ratios of AuNRs could be controlled by changing the concentration of $AgNO_3$ and ascorbic acid. The TEM micrograph of AuNRs (Fig. 1A) shows that the AuNRs are monodispersed. Analysis using Digital Micrograph software provided an average length of ca. 42.0 nm, width of ca. 10.2 nm, and aspect ratio of ca. 4.1. Coating MS shell produced a clear light contrast encapsulation on the AuNRs core (Fig. 1B). The MS shell was homogeneous and uniform with a thickness of ca. 33.7 nm. The diameter of the AuNRs@MS nanoparticles is ca. 85 nm. The UV–Vis spectra of the nanoparticle suspensions are shown in Fig. S-1 (Supplementary Material). The as-synthesized AuNRs exhibited a weak transverse plasmon band at around 512 nm and a strong longitudinal plasmon band at 819 nm. After being coated with the MS shell, the longitudinal plasmon band exhibited a slight red shift (~8 nm) because the silica shell increases the local refractive index of the medium surrounding the AuNRs (Fang et al., 2016; Zhang et al., 2008).

3.2. Probing the biosensor fabrication process

The surface morphology of the GC electrode after each fabrication step was probed by SEM (Fig. 2). The 'AuNRs@MS'@TiO_2-CS casting (Fig. 2A) introduced a mesoporous and homogeneous base layer, among which nanoparticles of ca. 85 nm in diameter are dispersed (pointed with arrows in the figure). The base layer is composed of interconnected nanoparticles of ca. 15 nm, and pores of ca. 5 nm in diameters. The morphology of the base layer is the same with that of the TiO_2-CS casting (Figure S-2A in Supplementary Material), while the dispersed nanoparticles are the doped AuNRs@MS. The size of the

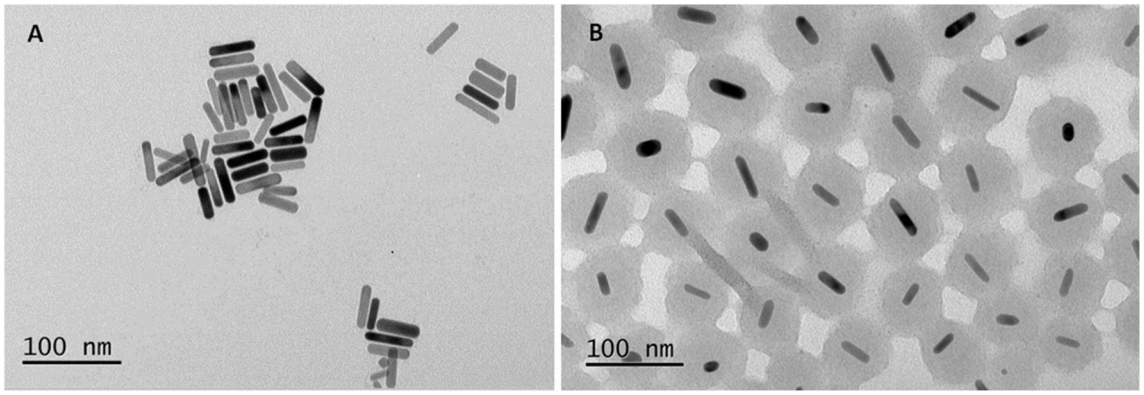

Fig. 1. (A, B) The TEM images of the as-synthesized (A) AuNRs and (B) AuNRs@MS.

doped nanoparticles is similar with that of the free AuNRs@MS nanoparticles (Fig. 1B), indicating a highly dispersive and homogeneous doping. However, a dispersive and homogeneous doping of bare AuNRs was also observed (Fig. 2B), which was out of our expectation. In our expriemental design, the coating of MS shell on the AuNRs was to prevent the AuNRs from aggregation in acidic TiO_2-CS colloidal solution. We therefore investigated the colloidal stability of bare AuNRs in both acidic and alkaline conditions. The UV–Vis spectra of the AuNRs solution after incubatin in 1 M HCl (Fig. S-3A) show that it is stable in acidic condition. On the contrary, alkaline condition induced the AuNRs aggration (Fig. S-3B). In AuNRs preparation, CTAB forms a bilayer around the AuNRs surface (Fang et al., 2016), protecting the AuNRs from aggregation in neutral and acidic conditions. In alkaline conditions, the ammonium group of CTAB was deprotonated, destroying the CTAB bilayer thus leading to the aggregation of AuNRs.

The electrodeposition of a CS layer on the 'AuNRs@MS'@TiO_2-CS sol-gel produced a quite bumpy surface (Fig. 2C). The sizes of the bumps are various, with some are as large as ca. 500 nm. In contrast,

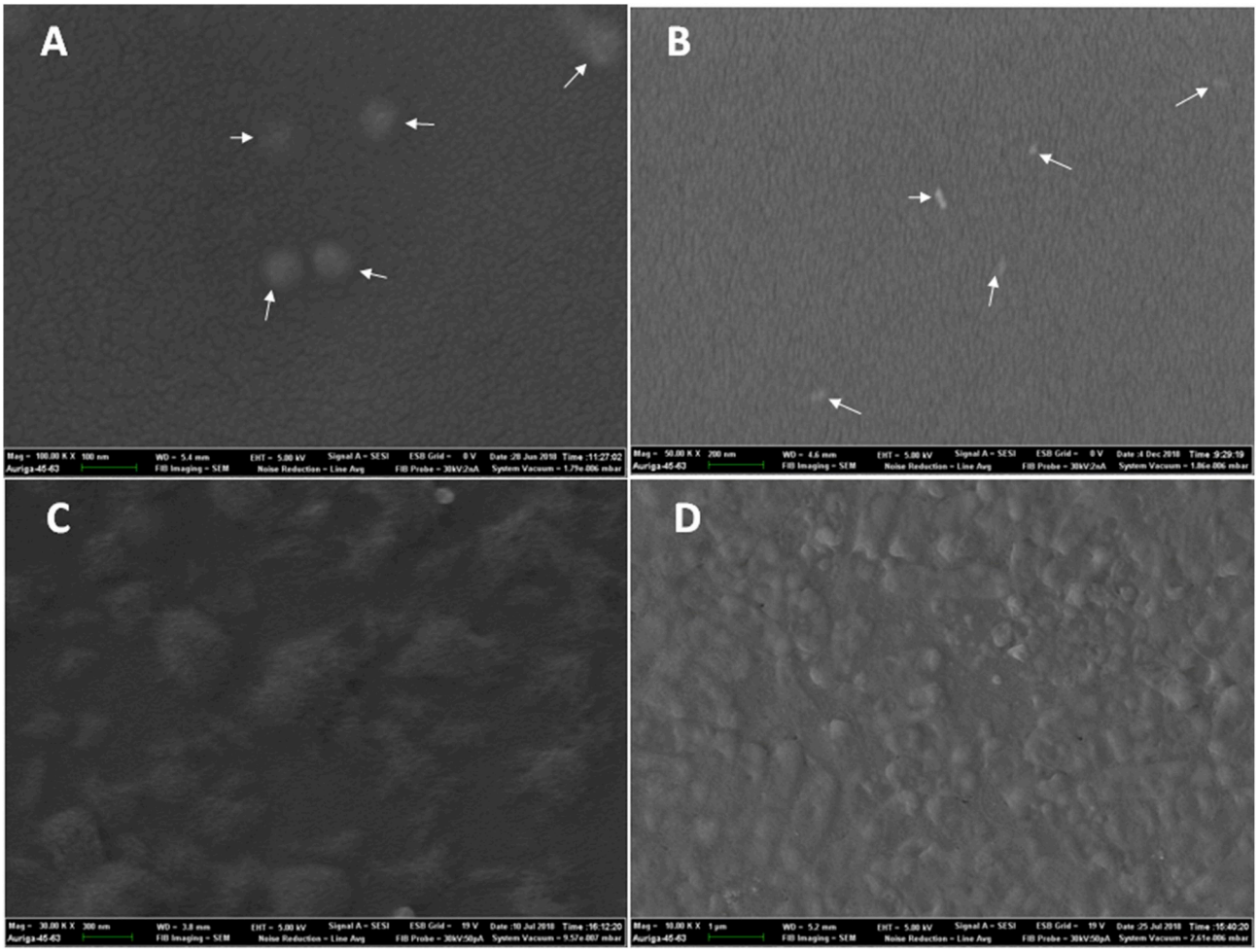

Fig. 2. The SEM images of (A) 'AuNRs@MS'@TiO_2-CS, (B) AuNRs@TiO_2-CS, (C) CS/'AuNRs@MS'@TiO_2-CS, and (D) AChE/CS/'AuNRs@MS'@TiO_2-CS modified GC electrodes. The concentration of the AuNRs@MS solution and the bare AuNRs solution in preration of the nanocomposites was 0.58 nM. The volume ratio of TiO_2 precursor solution to AuNRs@MS solution or to bare AuNRs solution was 90:10.

the surface of the bumps is mesoporous and the border of the bumps is fibrous. This surface morphology is quite different with the relatively flat surfaces of that without AuNRs@MS doping (Fig. S-2B) (Cui et al., 2018), and of that with the bare AuNRs doping (Fig. S-2C). Doping of AuNRs@MS nanoparticles may cause inhomogeneous micro-distribution of electroconductivity and electrocatalytic activity in the hydrogel, which in turn causes inhomogeneous electrodeposition of the CS layer. The bumpy surface, in addition to the mesoporous and fibrous nanostructure should be beneficial for the following AChE immobilization, via providing a large surface area. After AChE immobilization (Fig. 2D), the surface is still bumpy, but the micro-surface becomes smoother, indicating that AChE loading fills the pores. However, it should be noted that the AChE loaded CS/'AuNRs@MS'@TiO_2-CS surface is still mesoporous (Fig. S-2D, higher magnification image). The mesoporous structure could allow small molecules, such as ATCl, TCl, and OPs to permeate through the matrix, facilitating the small molecules to efficiently contact with the immobilized enzyme, the doped AuNRs, as well as the underneath GC electrode.

The biosensor fabrication process was also probed by electrochemical techniques. With $K_3[Fe(CN)_6]$ as probe (Fig. 3A), a symmetric pair of peaks with E_0' of about +0.267 V from the redox reactions of the probe were observed at all the electrodes. Introduction of the 'AuNRs@MS'@TiO_2-CS nanocomposite (curve b) drastically decreased

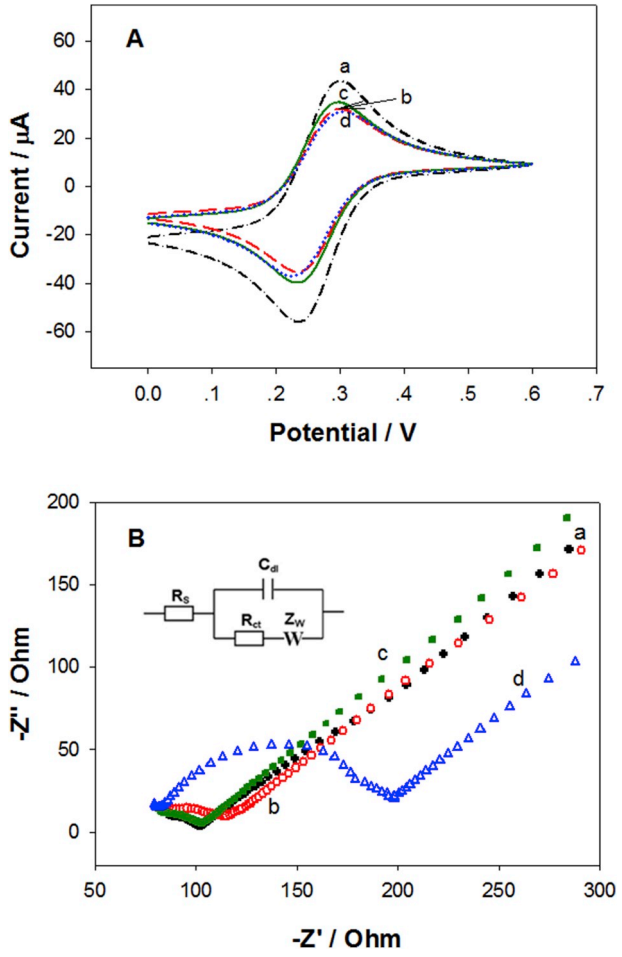

Figure 3. (A) The CVs, and (B) the Nyquist plots of (a) GC, (b) 'AuNRs@MS'@TiO_2-CS/GC, (c) CS/'AuNRs@MS'@TiO_2-CS/GC, and (d) AChE/CS/'AuNRs@MS'@TiO_2-CS/GC electrodes, in (A) 5 mM $K_3[Fe(CN)_6]$ (scan rates: 0.05 V s^{-1}), and (B) $[Fe(CN)6]^{3-/4-}$ (10/10 mM). Inset in B: the Randles equivalent circuit model. The concentration of AuNRs@MS suspension was 0.58 nM. The volume ratio of TiO_2 precursor solution to AuNRs@MS solution was 90:10.

the redox currents, owing to the semi-conductivity of TiO_2, the non-conductivity of CS, and the negative charges of the TiO_2 gel. In contrast, the electrodeposition of the CS film on 'AuNRs@MS'@TiO_2-CS (curve c) obviously increased the redox currents. The positive charges of the CS film adsorb and accumulate the negative-charged $K_3[Fe(CN)_6]$ probe molecules, resulting in the increment of the redox currents. As expected, the immobilization of AChE (curve d) leaded to the decrement of the redox currents, due to its non-conductive and negative-charge property. The EIS technique, which can provide the information of membrane capacitance and resistance, provided similar results. As shown in Fig. 3B, the Nyquist complex plane plots of the electrodes exhibit a single semicircle at high frequency domain and a straight line at low frequency domain. The linear tail with a slope of unity is dominated by the interfacial mass transfer of the redox species, while the semicircle impedance is mainly contributed by the charge-transfer resistance (R_{ct}) and the double-layer capacitance (C_{dl}) of the electrode surface. The R_{ct} values were determined by ZSimpWin (Princeton Applied Research) using a modified Randles circuit (Inset in Fig. 3B). For the bare GC (curve a), 'AuNRs@MS'@TiO_2-CS/GC (curve b), CS/'AuNRs@MS'@TiO_2-CS/GC (curve c), and AChE/CS/'AuNRs@MS'@TiO_2-CS/GC (curve d) electrodes, the R_{ct} value was 24.7 Ω, 63.6 Ω, 33.6 Ω, and 124.5 Ω respectively. With higher R_{ct} value reflecting worse charge-transfer rate, the results of the R_{ct} value are consistent with the above CV results.

3.3. Effect of AuNRs@MS doping and mechanism investigation

The effect of the AuNRs@MS doping was investigated by comparing the DPV curves of the biosensor with various immobilization matrix components in 1 mM ATCl (Fig. 4A). For all the biosensors, a strong oxidation peak appeared at the potential of ca. 0.65 V, coming from the electro-oxidation of the enzymatic product TCl. This result indicates that the immobilized AChE is bioactive, transforming ATCl to TCl, and TCl can be electro-oxidized at the electrode (Scheme 1). The biosensor with the AuNRs@MS doping (curve d) exhibited a significantly larger DPV peak (peak current, I_{cat}, ~3.09 μA) than those without any doping (curve a, incorporation of water, I_{cat} = ~1.41 μA; curve b, incorporation of the TiO_2 sol-gel instead, I_{cat} = ~1.59 μA). In contrast, although doping of bare AuNRs (curve c, I_{cat} = ~1.84 μA) obviously increased the DPV response in comaprions with those without any doping, its enhancement effect is drastically lower than the AuNRs@MS doping. The above SEM measurement showed that both AuNRs@MS and bare AuNRs nanoparticles are dispersed homogeneously inside the TiO_2-CS gel. Then the mechanisms for their variations in bioelectrocatalytic activity was investigated by EIS measurment. Fig. 4B illustrates the EIS spectra of the corresponding electrodes without the CS film deposition and the AChE loading. Doping AuNRs@MS nanoparticles (curve d) significantly enhanced the electrode charge-transfer rate, reflected by the significant decrement of the R_{ct} value from 380 Ω (water incorporated TiO_2-CS gel, curve a) and 333 Ω (TiO_2 incorporated TiO_2-CS gel, curve b) to 77 Ω. In contract, doping bare AuNRs only decreased the R_{ct} value to 253 Ω. The R_{ct} value of the AuNRs@MS doped TiO_2-CS hydrogel was drastically smaller than that of the bare AuNRs counterpart, indicating a significantly stronger enhancement of the electrode electroconductivity. The exact reason for the higher electroconductiviy is not clear at this moment. Herein we propose that the AuNRs@MS doping results in electron tunnling between the doped AuNRs@MS nanoparticles, most possibly contributed by the mesoporous structure of the MS shell on the AuNRs. This proposed mechanism could also explain the bumpy and fibrous surface mporpholgy of the CS film electrodeposited 'AuNRs@MS'@TiO_2-CS/GC electrode. Electron tunneling between the doped AuNRs@MS nanoparticles could result in higher CS electrodeposition current at specific electron tunnling channels. The exact mechanism for the enhanced electroconductivity needs further invesigations. The enhancement of electroconductivity with the AuNRs@MS doping should be one of the main reasons for the improved

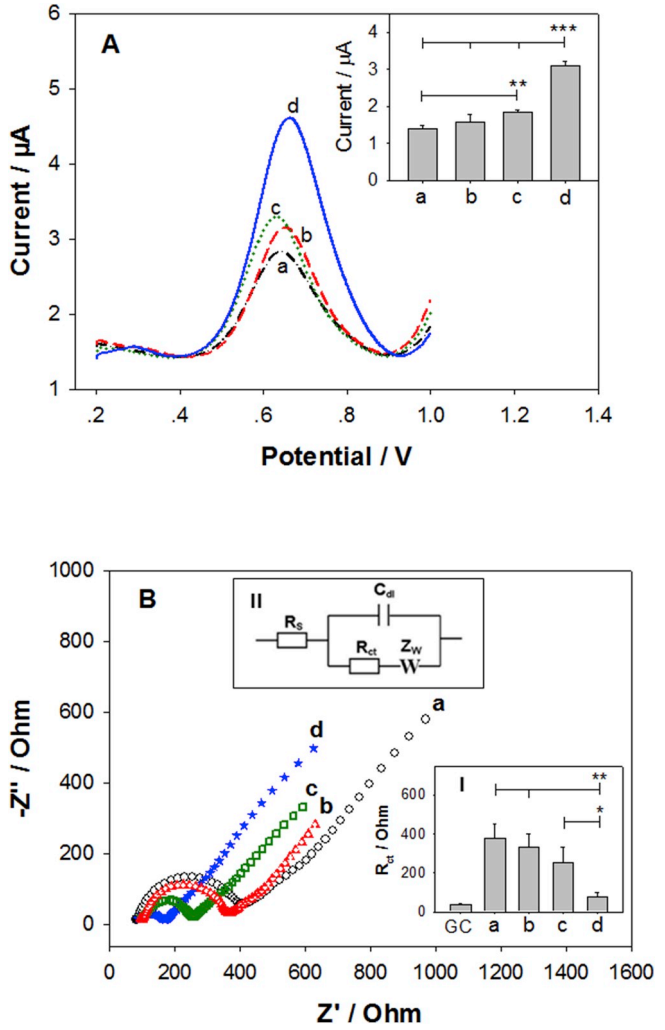

Figure 4. (A) DPV curves of (a) AChE/CS/H_2O@TiO_2-CS/GC, (b) AChE/CS/TiO_2-CS/GC, (c) AChE/CS/AuNRs@TiO_2-CS/GC, and (d) AChE/CS/'AuNRs@MS'@TiO_2-CS/GC electrodes in PBS containing 1 mM ATCl. Inset in A: the corresponding statistic I_{cat} values of the DPV curves. (B) The EIS of (a) H_2O@TiO_2-CS/GC, (b) TiO_2-CS/GC, (c) AuNRs@TiO_2-CS/GC, and (d) 'AuNRs@MS'@TiO_2-CS/GC electrodes in $[Fe(CN)6]^{3-/4-}$ (10/10 mM). Inset I in B: the corresponding statistic R_{ct} values obtained from the EIS spectra. Inset II in B: the Randles equivalent circuit model. The concentratios of AuNRs@MS suspension and AuNRs suspension were 0.58 nM. The volume ratio of TiO_2 precursor solution to AuNRs@MS suspension (or AuNRs suspension, or H_2O) was 90:10. ***, **, and * represents that the p value is less than 0.001, 0.01, and 0.05, respectively in the *t*-test (independent biosensor preparations, n = 3).

bioelectrocatalytic activity of the as-fabricated AChE biosensor. The enhanced bioelectrocatalytic activity should also be contributed by high electrocatalytic activity of AuNRs, and a more efficient AChE loading on the bumpy and fibrous CS/'AuNRs@MS'@TiO_2-CS/GC surface.

3.4. Optimization of the biosensor

The electrodeposition time for the CS layer, and the loading concentration of AChE have been optimized in our previous biosensor fabrication (Cui et al., 2018). In this study, the AuNRs@MS doping amount was optimized. Firstly, when the volume ratio of the TiO_2 precursor solution to the AuNRs@MS solution was kept at 90:10, the concentration of the AuNRs@MS solution was varied from 0.19 nM to 0.96 nM (Fig. S-4A). It was found that 0.58 nM AuNRs@MS suspension resulted in an optimum 'AuNRs@MS'@TiO_2 nanocomposite hydrogel for the AChE biosensor fabrication. Afterwards, the volume ratio of the TiO_2 precursor solution to the 0.58 nM AuNRs@MS soultion was varied from 92:8 to 86:14 (Fig. S-4B). The optimum ratio was determined to be 90:10.

3.5. Bioelectrocatalytic activity and analytical performances

The bioelectrocatalytic activity of the optimum AChE biosensor was investigated by recording the DPV curves in a series of different concentrations of ATCl (Fig. S-5). The I_{cat} value increased monotonically with the ATCl concentration changing from 0.1 to 9 mM. The bioelectrocatalytic response follows the Michaelis–Menten kinetics. A linear $1/I_{cat}$ (μA^{-1}) vs. $1/C_{ATCl}$ (mM^{-1}) plot (Inset in Fig. S-5) was obtained. By using the Lineweaver-Burk equation (Eq. (2)), the apparent Michaelis–Menten constant (K_m) was obtained to be 1.89 mM. This K_m value is obviously smaller than that of our previously reported AChE biosensor (K_m = 3.1 mM) (Cui et al., 2018). The previous AChE biosensor was based on graphene modified GC electrode. The lower K_m value in this paper indicates that doping AuNRs@MS nanoparticles obviouly enhances the bioelectrocatalytic activity of the biosensor. However, we found that graphene modification on GC electrode and AuNRs@MS doping inside TiO_2-CS hydrogel could not achieve synergic effect. The exact reason is not understood at this moment.

$$\frac{1}{I_{cat}} = \frac{K_m}{I_{max}} \times \frac{1}{C_{ATCl}} + \frac{1}{I_{max}} \quad (2)$$

The analytical performances of the enzyme biosensor was then evaluated with DDVP and fenthion as model OPs molecules. Fig. 5 illustrates the DPV curves in 1 mM ATCl without incubating the biosensor with DDVP (curve a, I_{cat}: ~3.31 μA), and after incubating the biosensors in various concentrations of DDVP (curve b to j). After incubating in DDVP, the I_{cat} value decreased gradually with the increase of the DDVP concentration (C_{DDVP}), and finally dropped to ~0.39 μA at 13.6 μM C_{DDVP}, due to the inhibition of AChE by DDVP. The plot of Inh % versus C_{DDVP} (Inset in Fig. 5) shows two linear ranges: from 0.018 μM (4.0 ppb) to 0.453 μM, and from 0.453 μM to 13.6 μM, with the regression equation of Inh% (%) = 8.59 + 129.84 × C_{DDVP} (μM), and Inh% (%) = 65.29 + 1.84 × C_{DDVP} (μM), and a regression coefficient of 0.9942 and 0.9944, respectively. The limit of detection (LOD) was 5.3 nM (1.2 ppb) (calculated in a 3σ rule, i.e. 3 × S.D. of blank sample

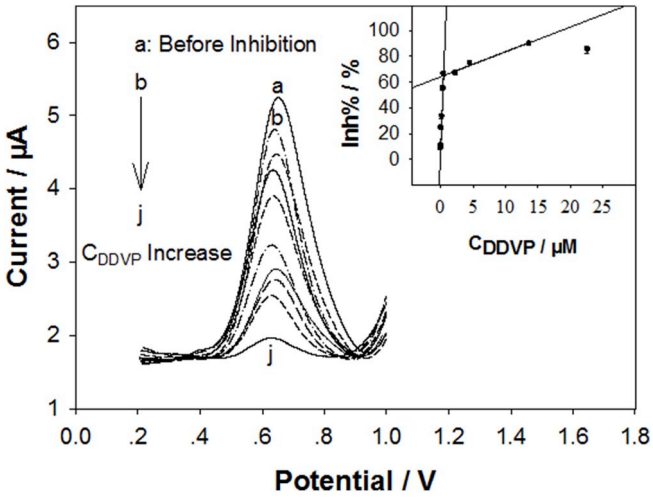

Fig. 5. The DPV curves of the AChE/CS/'AuNRs@MS'@TiO_2-CS/GC electrodes in 1 mM ATCl, without incubating the electrode with DDVP (curve a), and after incubating the electrodes in various concentrations of DDVP (from curve b to j, the DDVP concentration was 0.018, 0.036, 0.091, 0.181, 0.362, 0.453, 2.26, 4.53, and 13.6 μM, respectively). Inset: the Inh% values for various concentrations of DDVP. The repetitive number (independent biosensor preparations) n = 3–4.

signals, n = 5). The detection sensitivity of the as-fabricated biosensor is markedly higher than that of our previously reported AChE biosensor (LOD for DDVP: 29 nM) (Cui et al., 2018). The biosensor in detecting fenthion (Fig. S-6) exhibited a similar result with the DDVP detection. The LOD value for fenthion was 1.3 nM (0.36 ppb). The biosensor sensitivity is also compared with those of other reported electrochemical AChE biosensors (Wei and Wang, 2015; Sundarmurugasan et al., 2016; Itoh et al., 2014; Guan et al., 2012; Yan et al., 2013; Kaur et al., 2015; Dutta and Puzari, 2014; Wu et al., 2013) (Tables S–1), and with those of traditional detection methods, such as gas chromatography–tandem mass spectrometry (GC–MS^2), liquid chromatography–tandem mass spectrometry (LC–MS^2), and enzyme-linked immunosorbent assay (ELISA) (Santos et al., 2018; Radišic et al., 2009; Srivastava et al., 2017; Navarro et al., 2013; Qian et al., 2009) (Tables S–2). The LOD value and the linear range of the biosensor are comparable to or superior than most of the reported values. It should be noted that for our biosensor, both the LOD value and the lowest value (4.0 ppb for DDVP) in the linear range are lower than the maximum residue limits (MRLs) (10 ppb for DDVP), as reported in the European Union pesticides database and those from the U.S. Department Agriculture. It should also be noted that the biosensor method doesn't need a sample pretreatment step, which is necessary for the traditional GC–MS^2 (Santos et al., 2018; Srivastava et al., 2017) and LC–MS^2 (Radišic et al., 2009) methods (Tables S–2). The detection specificity of the biosensor was evaluated with fructose, glucose, sucrose, and ascorbic acid as interferents (Fig. S-7). The interferents tested did not induce obviously higher Inh% than blank PBS, indicating a high OPs detection specificity with the biosensor.

The as-fabricated biosensor is very reproducible, reflected by low Relative Standard Deviation (RSD) value for OPs detection with independent biosensor preparations. For example, the Inh% for 4.53 μM fenthion with 4 independent biosensor preparations was 63.38% ± 2.02% (mean ± S.D.), with an RSD value of only 3.2%. Same to our previously reported AChE biosensor (Cui et al., 2018), the most amazing property of the AuNRs@MS nanoparticle doped CS/TiO_2-CS hydrogel based enzyme biosensor is excellent stability, which is a very important character for practical applicability. Firstly, the biosensor is very stable during detection. The RSD value of the sensing signals in response to 1 mM ATCl (i.e. I_{cat}) during different detection time points in 9–21 min ATCl incubation time was ~2.2% (Fig. S-8). Secondly, the storage stability of the biosensor is very high. After the storage at dry (−20 °C) or wet (−4 °C) conditions for 30 days, the signal intensities of the biosensors kept 96% or 98% of the original values, respectively (Fig. S-9). By keeping the advantage of high stability of our AChE/CS/TiO_2-CS/rGO biosensor (Cui et al., 2018) (Tables S–3), the as-prepared AChE biosensor in this work shows higher storage stability than most of the reported AChE electrochemical biosensors (Tables S–3). The very excellent stability is attributed to both the incorporation and electrodeposition of CS into/on the TiO_2 immobilization matrix. CS not only strengthens the TiO_2 film and also reinforces the AChE immobilization through electrostatic interaction (Scheme 1).

Finally, the applicability of the biosensor was evaluated (Tables S–4). For the fenthion added in the cabbage juice samples, the recovery ratios were all within the range of 100 ± 5%, the RSDs were less than 12.0%, indicating a very accurate OPs detection.

4. Conclusions

AuNRs@MS core-shell nanoparticles were doped in mesoporous TiO_2-CS hydrogel simply by mixing the nanoparticle suspension with TiO_2 precursor solution right before being cast on electrode for gelation. The AuNRs@MS nanoparticles are dispersed homogeneously in the TiO_2-CS hydrogel. Doping AuNRs@MS nanoparticles significantly enhances the electro-conductivity of the TiO_2-CS hydrogel, and the bioelectrocatalytic activity of the AChE immobilized CS/TiO_2-CS matrix. In addition, with the AuNRs@MS doping, electrodeposition of CS film resulted in a bumpy and fibrous matrix surface. The mesoporous, bumpy, and fibrous matrix could facilitate AChE loading, and allow permeation of small molecules into/through the matrix. Consequently, the OPs detection sensitivity of the AuNRs@MS doped AChE biosensor is significantly enhanced compared with the bare AuNRs doped as well as the non-doping counterparts. The developed AChE biosensor shows high stability, sensitivity, reproducibility, and accuracy in detecting OPs. With the high performance of the AChE biosensor, our future work will focus on controlling the gelation time of TiO_2 sol-gel based matrix, and developing a disposable and applicable AChE biosensor for OPs detection.

CRediT authorship contribution statement

Hui-Fang Cui: Conceptualization, Funding acquisition, Supervision, Data curation, Formal analysis, Writing - original draft, Writing - review & editing. **Ting-Ting Zhang:** Data curation, Formal analysis, Investigation, Methodology, Writing - original draft. **Qi-Yan Lv:** Validation, Investigation. **Xiaojie Song:** Software, Data curation. **Xiao-Jing Zhai:** Formal analysis, Investigation. **Gai-Gai Wang:** Investigation.

Acknowledgements

This work was supported by Plan for Scientific Innovation Talent of Henan Province to H. F. Cui (Grant number 154200510007), the National Natural Science Foundation of China (Grant number NSFC 21345007), the Provincial Natural Science Foundation of Henan (Grant number 182300410314), and the Henan Open-up and Collaboration Program of Science and Technology (Grant number 132106000070).

Appendix A. Supplementary data

Supplementary data to this article can be found online at https://doi.org/10.1016/j.bios.2019.111452.

References

Behera, S.S., Das, U., Kumar, A., Bissoyi, A., Singh, A.K., 2017. Int. J. Biol. Macroml. 98, 329–340.
Chang, Y.T., Liao, P.Y., Sheu, H.S., Tseng, Y.J., Cheng, F.Y., Yeh, C.S., 2012. Adv. Mater. 24, 3309–3314.
Choi, W.I., Sahu, A., Kim, Y.H., Tae, G., 2012. Ann. Biomed. Eng. 40, 534–546.
Costa, L.G., 2006. Clin. Chim. Acta 366, 1–13.
Cui, H.F., Zhang, K., Zhang, Y.F., Sun, Y.L., Wang, J., Zhang, W.D., Luong, J.H., 2013. Biosens. Bioelectron. 46, 113–118.
Cui, H.F., Xu, T.B., Sun, Y.L., Zhou, A.W., Cui, Y.H., Liu, W., Luong, J.H.T., 2015. Anal. Chem. 87, 1358–1365.
Cui, H.F., Wu, W.W., Li, M.M., Song, X.J., Lv, Y.X., Zhang, T.T., 2018. Biosens. Bioelectron. 99, 223–229.
Dutta, R.R., Puzari, P., 2014. Biosens. Bioelectron. 52, 166–172.
Eddleston, M., Buckley, N.A., Eyer, P., Dawson, A.H., 2008. Lancet 371, 597–607.
Fang, S., Li, C.X., Lin, J., Zhu, H.G., Cui, D.X., Xu, Y.S., Li, Z.M., 2016. J. Nanomater. 2016, 1082746.
Guan, H., Zhang, F., Yu, J., Chi, D., 2012. Food Res. Int. 49, 15–21.
Hill, H.D., Vega, R.A., Mirkin, C.A., 2007. Anal. Chem. 79, 9218–9223.
Itoh, T., Shimomura, T., Hayashi, A., Yamaguchi, A., Teramae, N., Ono, M., Tsunoda, T., Mizukami, F., Stucky, G.D., Hanaoka, T.A., 2014. Analyst 139, 4654–4660.
Kaur, B., Srivastava, R., Satpati, B., 2015. ChemElectroChem 2, 1164–1173.
Li, G.J., Li, X.L., Wan, J., Zhang, S.S., 2009. Biosens. Bioelectron. 24, 3281–3287.
Long, Q., Li, H.T., Zhang, Y.Y., Yao, S.Z., 2015. Biosens. Bioelectron. 68, 168–174.
Lu, L.L., Xia, Y.S., 2015. Anal. Chem. 87, 8584–8591.
Ma, L., Zhou, L.Y., He, Y., Wang, L.H., Huang, Z.H., Jiang, Y.J., Gao, J., 2018. Electroanalysis 30, 1793–1802.
Mostafalou, S., Abdollahi, M., 2017. Arch. Toxicol. 91, 549–599.
Nam, J.M., Stoeva, S.I., Mirkin, C.A., 2004. J. Chem. Am. Soc. 126, 5932–5933.
Navarro, P., Perez, A.J., Gabaldon, J.A., Nunez-Delicado, E., Puchades, R., Maquieira, A., Morais, S., 2013. Talanta 116, 33–38.
Nikoobakht, B., El-Sayed, M.A., 2003. Chem. Mater. 15, 1957–1962.
Orendorff, C.J., Murphy, C.J., 2006. J. Phys. Chem. B 110, 3990–3994.
Patocka, J., Kuca, K., Jun, D., 2004. Acta Med. 47, 215–228.
Qian, G.L., Wang, L.M., Wu, Y.R., Zhang, Q., Sun, Q., Liu, Y., Liu, F.Q., 2009. Food Chem. 117, 364–370.
Qian, S.H., Lin, H.W., 2015. Anal. Chem. 87, 5395–5400.

Radišic, M., Grujic, S., Vasiljevic, T., Lauševic, M., 2009. Food Chem. 113, 712–719.
Santos, C., Oppolzer, D., Gonçalves, A., Barroso, M., Gallardo, E., 2018. J. Anal. Toxicol. 42, 321–329.
Shi, M.H., Xu, J.J., Zhang, S., Liu, B.H., Kong, J.L., 2006. Talanta 68, 1089–1095.
Srivastava, N., Kumari, S., Nair, K., Alam, S., Raza, S.K., 2017. J. AOAC Int. 100, 804–809.
Sundarmurugasan, R., Gumpu, M.B., Ramachandra, B.L., Nesakumar, N., Sethuraman, S., Krishnan, U.M., Rayappan, J.B.B., 2016. Sensor. Actuator. B Chem. 230, 306–313.
Tang, Y.J., Hu, X.L., Zhang, X.Q., Guo, D.L., Zhang, J.H., Kong, F.G., 2016. Carbohydr. Polym. 1519, 752–759.
Varmira, K., Mohammadi, G., Mahmoudi, M., Khodarahmi, R., Rashidi, K., Hedayati, M., Goicoechea, H.C., Jalalvand, A.R., 2018. Talanta 183, 1–10.
Wang, H.F., Huff, T.B., Zweifel, D.A., He, W., Low, P.S., Wei, A., Cheng, J.X., 2005. Proc. Natl. Acad. Sci. U.S.A. 102, 15752–15756.
Wei, M., Wang, J.J., 2015. Sensor. Actuator. B Chem. 211, 290–296.
Wu, S., Huang, F., Lan, X., Wang, X., Wang, J., Meng, C., 2013. Sensor. Actuator. B Chem. 177, 724–729.
Yan, J., Guan, H., Yu, J., Chi, D., 2013. Pestic. Biochem. Physiol. 105, 197–202.
Yang, G.H., Su, J.F., Guo, Y.P., Xu, H., Ke, Q.F., 2017. J. Mater. Sci. 52, 5404–5416.
Yu, J.H., Ju, H.X., 2002. Anal. Chem. 74, 3579–3583.
Yu, G.X., Wu, W.X., Zhao, Q., Wei, X.Y., Lu, Q., 2015. Biosens. Bioelectron. 68, 288–294.
Zhang, J.J., Liu, Y.G., Jiang, L.P., Zhu, J.J., 2008. Electrochem. Commun. 10, 355–358.
Zhu, Y.H., Cao, H.M., Tang, L.H., Yang, X.L., Li, C.Z., 2009. Electrochim. Acta 54, 2823–2827.